

Quantum Science and Technology



PAPER

Resonator-mediated quantum gate between distant charge qubits

OPEN ACCESS

RECEIVED
10 June 2024

REVISED
14 August 2024

ACCEPTED FOR PUBLICATION
4 September 2024

PUBLISHED
19 September 2024

Original Content from
this work may be used
under the terms of the
[Creative Commons
Attribution 4.0 licence](#).

Any further distribution
of this work must
maintain attribution to
the author(s) and the title
of the work, journal
citation and DOI.



Florian Kayatz , Jonas Mielke and Guido Burkard*

Department of Physics, University of Konstanz, D-78457 Konstanz, Germany

* Author to whom any correspondence should be addressed.

E-mail: guido.burkard@uni-konstanz.de

Keywords: circuit quantum electrodynamics, double quantum dot charge qubit, entangling two-qubit gate, semiconductor, long distance interaction

Abstract

Strong charge-photon coupling allows the coherent coupling of a charge qubit, realized by a single charge carrier (either an electron or a hole) in a double quantum dot, to photons of a microwave resonator. Here, we theoretically demonstrate that, in the dispersive regime, the photons can mediate both an i SWAP gate as well as a \sqrt{i} SWAP gate between two distant charge qubits. We provide a thorough discussion of the impact of the dominant noise sources, resonator damping and charge qubit dephasing on the average gate fidelity. Assuming a state-of-the-art resonator decay rate and charge qubit dephasing rate, the predicted average gate fidelities are below 90%. However, a decrease of the charge qubit dephasing rate by one order of magnitude is conjectured to result in gate fidelities surpassing 95%.

1. Introduction

The advanced production methods in the microelectronics industry, in particular for semiconductors such as Si, paved the way for electrostatically defined Si/SiGe quantum dots (QD) and arrays of such QDs [1–5] with excellent control over the individual QD potentials thereby demonstrating the high capability for scaling in this quantum computing hardware approach. There are different ways to implement a qubit using quantum dots. For an electron confined in a QD, the spin [6, 7] or the valley [8–10] degree of freedom are utilized to operate a qubit. Likewise, the spin of a confined hole can define the qubit states [11]. On the other hand, combining two nearby QDs to a double quantum dot (DQD) opens up the possibility for further qubit implementations. The most basic among these is the charge qubit [12–16] obtained by filling a DQD with a single charge carrier, either an electron or a hole. The same single charge carrier configuration can also be used to realize the flopping mode spin qubit [17–19]. The addition of a second electron or hole to the DQD allows for various types of singlet-triplet qubits [20–25].

Regardless of the specific qubit realization, building a quantum computer requires excellent control over the individual qubits in the form of single-qubit gates and the possibility to couple two qubits via entangling two-qubit gates such as the prominent CNOT gate, the i SWAP gate, as well as the \sqrt{i} SWAP gate. The availability of an entangling two-qubit gate is essential for quantum computing because in combination with single-qubit gates arbitrary multi-qubit operations can be performed [26]. The aforementioned two-qubit gates are effectively equivalent to the CNOT operation, as this operation can be constructed using a combination of single-qubit gates and either i SWAP gates [27] or \sqrt{i} SWAP gates [28, 29]. The set of intrinsic two-qubit gates available in a specific device is determined by its physical properties. For example, systems with an XY-interaction can implement intrinsic i SWAP and \sqrt{i} SWAP gates [30].

For the practical implementation of quantum computation and quantum error correction, long-range coupling between distant qubits is highly desirable. An ideal situation would be the availability of ‘all-to-all’ connectivity [31, 32], i.e. an architecture with connectivity between any desired pair of qubits. The direct coupling between electrons, such as the capacitive coupling [33–38] and exchange [39–43], can be harnessed to build two-qubit gates in semiconductor devices. However, these interactions are typically short-ranged and do not allow the coupling of distant qubits. There are various approaches to couple distant qubits including the physical shuttling of qubits [44–58], an inter-qubit coupling mediated by a ‘jellybean’ quantum

dot [59–64], and adiabatic passage protocols [65–73]. Another promising approach is the circuit quantum electrodynamics architecture (cQED), as considered in this paper, where a microwave resonator acts as a mediator between spatially separated qubits.

Circuit quantum electrodynamics architectures were initially established in the field of superconducting qubits [74, 75]. However, many of these concepts are also applicable to other systems [76] including semiconductor-based qubits [77]. Strong charge-photon coupling and strong spin-photon coupling [78–83] have been realized in circuit quantum electrodynamics with semiconductor devices in the past few years. Therefore, microwave resonators constitute such an intermediate system and have proven to implement a coupling between charge qubits separated by 42 μm in the resonant and dispersive charge-photon coupling regime [84] as well as the coupling between spins separated by more than four millimeters in the resonant [81] and the dispersive [82] spin-photon coupling regime. This result suggests that resonator-mediated two-qubit gates are within reach. In particular, a resonator-mediated i SWAP gate between spin qubits was suggested [85] and has recently been demonstrated [86]. The mechanism generating spin-photon coupling relies on spin-charge hybridization due to a magnetic field gradient in case of electrons and intrinsic spin-orbit coupling in case of holes, and thus couples spin and photons via the charge-photon dipole coupling [78, 79, 83, 85]. Therefore, the spin coherence time suffers from the charge admixture, while the spin-photon coupling strength is significantly reduced compared to the charge-photon one [78, 83]. Working in the strong-coupling regime of circuit QED with spin qubits thus requires a balance between spin-charge hybridization and spin coherence. Here, we study the simpler case of pure charge qubits that allow for strong coupling and short gate times at the expense of significantly lower coherence times. Moreover, in case of electrons, the absence of micromagnets significantly simplifies the device design.

We theoretically demonstrate that microwave resonator photons can mediate both an i SWAP gate as well as a \sqrt{i} SWAP gate between distant charge qubits defined in a single charge carrier DQD and dispersively coupled to the resonator. To assess the potential of the gate for quantum computation, the effects of resonator photon decay and charge qubit dephasing on the gate fidelity are systematically discussed. Assuming a state-of-the-art resonator decay rate and charge-qubit dephasing rate, the predicted average gate fidelities are below 90%. However, a decrease of the charge qubit dephasing rate by one order of magnitude is conjectured to result in gate fidelities surpassing 95%.

2. Model

We consider two ($i = 1, 2$) Si/SiGe DQDs each populated with a single charge carrier (figure 1), either an electron or a hole. The respective charge carrier can either be confined to the $|L^{(i)}(\text{eft})\rangle$ or $|R^{(i)}(\text{ight})\rangle$ QD of the DQD. The energy difference between the levels of the two QDs is parameterized by the detuning parameter $\varepsilon^{(i)}$, while the QDs are tunnel-coupled with coupling strength $t_c^{(i)}$. Thus, the dynamics of the individual DQDs are described by the Hamiltonian

$$\tilde{H}_{\text{DQD}}^{(i)} = \frac{\varepsilon^{(i)}}{2} \tilde{\tau}_z^{(i)} + t_c^{(i)} \tilde{\tau}_x^{(i)}, \quad (1)$$

with the position space Pauli operators $\tilde{\tau}_j^{(i)}$ defined by $\tilde{\tau}_z^{(i)} |L^{(i)}(R^{(i)})\rangle = \pm |L^{(i)}(R^{(i)})\rangle$.

Being interested in long-ranged resonator-mediated two-qubit gates, we look at a setup where both DQDs are coupled to the same mode of a microwave resonator with frequency ω_c . The Hamiltonian for the relevant resonator mode reads

$$H_c = \omega_c \left(a^\dagger a + \frac{1}{2} \right), \quad (2)$$

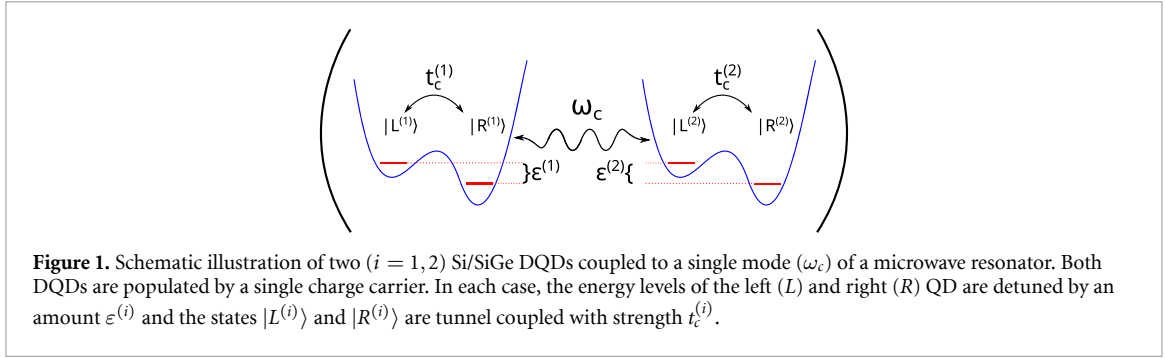
with a and a^\dagger the resonator photon annihilation and creation operators, respectively. Each single charge carrier DQD has a substantial electric dipole moment (dipole operator $\propto \tilde{\tau}_z^{(i)}$) resulting in an electric dipole interaction between the DQD charge degree of freedom and the resonator photons [77, 87],

$$\tilde{H}_{\text{int}}^{(i)} = g_c (a + a^\dagger) \tilde{\tau}_z^{(i)}. \quad (3)$$

In recent experiments a coupling strength of $g_c/2\pi \approx 513$ MHz for a hole-charge qubit was reported [83].

3. Entangling two-qubit gates

In this section, we derive an effective Hamiltonian describing the resonator-mediated interaction between two charge qubits and assess the potential of this interaction for quantum information applications. As a first



step, the states constituting the individual charge qubits are set as the two eigenstates of $\tilde{H}_{\text{DQD}}^{(i)}$,

$$|+\rangle^{(i)} = \cos\frac{\theta^{(i)}}{2}|L^{(i)}\rangle + \sin\frac{\theta^{(i)}}{2}|R^{(i)}\rangle, \quad (4)$$

$$|-\rangle^{(i)} = \sin\frac{\theta^{(i)}}{2}|L^{(i)}\rangle - \cos\frac{\theta^{(i)}}{2}|R^{(i)}\rangle, \quad (5)$$

with the orbital angle $\theta^{(i)}$ defined by $\tan\theta^{(i)} = 2t_c^{(i)}/\varepsilon^{(i)}$. The corresponding eigenvalues are

$$\pm\Omega^{(i)}/2 = \pm\frac{1}{2}\sqrt{(\varepsilon^{(i)})^2 + (2t_c^{(i)})^2}, \quad (6)$$

and in this basis the interaction between resonator and qubit $\tilde{H}_{\text{int}}^{(i)}$ reads

$$H_{\text{int}}^{(i)} = g_c (a + a^\dagger) \left(\sin\theta^{(i)}\tau_x^{(i)} + \cos\theta^{(i)}\tau_z^{(i)} \right), \quad (7)$$

where the Pauli matrices $\tau_j^{(i)}$ operate on the qubit states as $\tau_z^{(i)}|\pm\rangle^{(i)} = \pm|\pm\rangle^{(i)}$. Equation (7) clearly shows that the transverse qubit-resonator interaction, represented by the term $\propto \tau_x^{(i)}$, can be switched on and off by modulating the DQD detuning $\varepsilon^{(i)}$ and the tunnel coupling strength $t_c^{(i)}$. This allows individual qubits to be decoupled from the resonator and placed into an idling mode.

Readout of an individual charge qubit can be achieved by decoupling it from the resonator and adiabatically modulating the DQD detuning towards a strong bias, resulting in a mapping of the state $|+\rangle^{(i)}$ ($|-\rangle^{(i)}$) to the state $|L^{(i)}\rangle$ or $|R^{(i)}\rangle$ ($|R^{(i)}\rangle$ or $|L^{(i)}\rangle$), depending on the specific form of the detuning pulse. The states $|L^{(i)}\rangle$ and $|R^{(i)}\rangle$ can then be differentiated by measuring the charge occupation of the individual quantum dots using a quantum point contact (QPC) [88], a single electron transistor (SET) [89], or radiofrequency gate sensors [90].

Alternatively, in a setup where the charge qubit of interest is dispersively coupled to the resonator while the second qubit is decoupled from the resonator, the DQD system can be measured directly in the basis $\{|+\rangle^{(i)}, |-\rangle^{(i)}\}$ by assessing the qubit state-dependent resonator frequency shift [91].

We note that the energy levels of symmetric DQDs ($\varepsilon^{(i)} = 0$) are to first order insensitive to fluctuations in the detuning $\varepsilon^{(i)}$, i.e. $(\partial\Omega^{(i)}/\partial\varepsilon^{(i)})|_{\varepsilon^{(i)}=0} = 0$. Thus, adjusting a DQD to $\varepsilon^{(i)} = 0$ means tuning the qubit to a charge-noise sweet spot [78]. In the following we consider identical qubits at zero detuning, i.e. $\varepsilon^{(i)} = \varepsilon = 0$ and $t_c^{(i)} = t_c$, unless noted otherwise. Then the interaction Hamiltonian $\tilde{H}_{\text{int}}^{(i)}$ (7) simplifies to

$$H_{\text{int}}^{(i)} = g_c (a + a^\dagger) \tau_x^{(i)}. \quad (8)$$

The basis change leaves H_c unaffected. Equation (8) already suggests that there is a second-order process coupling the states $|+, -\rangle$ and $|-, +\rangle$, where $|i, j\rangle$ indicates the state of charge qubit 1 and 2, respectively, as given by i and j .

The charge qubits are resonant with the resonator mode if $\Omega = 2t_c = \omega_c$. Here, we focus on the dispersive regime $|2t_c - \omega_c| \gg g_c$ and low temperatures such that the resonator is empty. In this regime we can derive an effective Hamiltonian by applying a Schrieffer–Wolff-transformation (see appendix A) to decouple the subspace with zero photons from the one with higher photon numbers. For the zero photon subspace, we find the effective two-qubit Hamiltonian,

$$\bar{H}_d = \sum_{i=1}^2 \frac{E}{2} \tau_z^{(i)} + g_{\text{eff}} \tau_x^{(1)} \tau_x^{(2)}, \quad (9)$$

with

$$E = 2t_c - \frac{g_c^2}{\omega_c - 2t_c} + \frac{g_c^2}{\omega_c + 2t_c}, \quad (10)$$

and the effective qubit-qubit coupling strength

$$g_{\text{eff}} = -\frac{g_c^2}{\omega_c - 2t_c} - \frac{g_c^2}{\omega_c + 2t_c}. \quad (11)$$

The dynamics generated by the diagonal terms of (9) can be captured by a transformation into the interaction picture with respect to $\sum_{i=1}^2 E\tau_z^{(i)}/2$. In this frame (9) reads

$$H = g_{\text{eff}} \left(\tau_+^{(1)} \tau_-^{(2)} + \tau_-^{(1)} \tau_+^{(2)} \right) + g_{\text{eff}} \left(e^{2iEt} \tau_+^{(1)} \tau_+^{(2)} + e^{-2iEt} \tau_-^{(1)} \tau_-^{(2)} \right). \quad (12)$$

The effective interaction between the two charge qubits described by the first term in equation (12) leads to two-qubit dynamics characterized by a time scale $\propto 1/g_{\text{eff}}$. In the dispersive regime one has $|2E| \approx |2(2t_c)| > |2t_c - \omega_c| \gg g_c$ and therefore $g_{\text{eff}} \ll g_c$ according to equation (11) as well as $g_{\text{eff}} \ll |2E|$ such that applying the rotating wave approximation (RWA) is justified. With the RWA applied the second term is neglected and it is straightforward to calculate the time evolution operator generated by the Hamiltonian (12),

$$U(t, 0) = \begin{pmatrix} 1 & 0 & 0 & 0 \\ 0 & \cos(g_{\text{eff}}t) & -i \sin(g_{\text{eff}}t) & 0 \\ 0 & -i \sin(g_{\text{eff}}t) & \cos(g_{\text{eff}}t) & 0 \\ 0 & 0 & 0 & 1 \end{pmatrix}, \quad (13)$$

with respect to the basis $\{|+, +\rangle, |+, -\rangle, |-, +\rangle, |-, -\rangle\}$. The time evolution for the particular evolution times

$$t_{\text{iSWAP}} = \pi/2|g_{\text{eff}}|, \quad (14)$$

and

$$t_{\sqrt{\text{iSWAP}}} = \pi/4|g_{\text{eff}}|, \quad (15)$$

results in

$$U(t_{\text{iSWAP}}, 0) = \begin{pmatrix} 1 & 0 & 0 & 0 \\ 0 & 0 & \pm i & 0 \\ 0 & \pm i & 0 & 0 \\ 0 & 0 & 0 & 1 \end{pmatrix}, \quad (16)$$

and

$$U(t_{\sqrt{\text{iSWAP}}}, 0) = \begin{pmatrix} 1 & 0 & 0 & 0 \\ 0 & 1/\sqrt{2} & \pm i/\sqrt{2} & 0 \\ 0 & \pm i/\sqrt{2} & 1/\sqrt{2} & 0 \\ 0 & 0 & 0 & 1 \end{pmatrix}, \quad (17)$$

respectively, where the the sign $-(+)$ is obtained for $g_{\text{eff}}/|g_{\text{eff}}| = +(-)1$.

The Makhlin invariants [92] of (16) and (17) are independent of the sign of the off-diagonal elements, and therefore the respective operations with opposite sign are similar up to single qubit rotations. Thus, we refer to (16) as an i SWAP gate and to (17) as an \sqrt{i} SWAP quantum gate.

4. Noise analysis

The qubits and the microwave resonator couple to their respective environment. Therefore, it is necessary to analyze the impact of processes resulting from these couplings on the gate performance in detail. Here, we provide a detailed discussion of the two dominant noise processes: resonator photon decay and charge qubit dephasing. The effect of both noise processes on the gate performance is analyzed by calculating the average gate fidelity \bar{F} introduced in [93] and briefly summarized in appendix B.

Charge qubit relaxation does not significantly impact gate fidelity. This is evidenced by reports of DQD charge qubit relaxation times $T_1 = 45 \mu\text{s}$ [94], while in our study, as detailed below, gate times range from a few nanoseconds to approximately 125 ns (see figure 3).

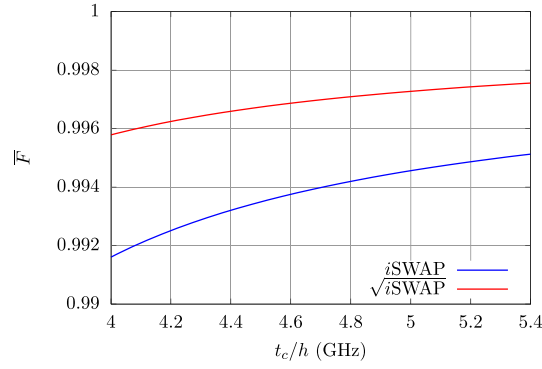


Figure 2. Average gate fidelity of the i SWAP (blue) and $\sqrt{i$ SWAP (red) quantum gates accounting for resonator damping as a function of the tunnel coupling strength t_c . Here $g_c/(2\pi) = 513$ MHz, $\omega_c/(2\pi) = 5.428$ GHz and $\kappa/(2\pi) = 14$ MHz are chosen [83].

4.1. Resonator damping

The interaction of the resonator with its environment is described by a coupling between the resonator mode and an electromagnetic bath. While, in practice, experiments are typically performed at cryogenic temperatures $T \leq 10$ mK [95], for simplicity, we assume that the environment is held at zero temperature. In this limit the environment resides in its ground state and the conservation of energy prohibits processes increasing the energy of the DQD-resonator system due to interactions with the environment. Moreover, there is no thermal population of the resonator, i.e. $\langle a^\dagger a \rangle = 0$. The reasoning we present in appendix C demonstrates that the dissipative dynamics due to resonator damping are described by the Lindblad master equation

$$\dot{\rho} = -i[H, \rho] + \frac{\kappa g_c^2}{(\omega_c - 2t_c)^2} \mathcal{D} \left[\tau_-^{(1)} + \tau_-^{(2)} \right] (\rho), \quad (18)$$

with the density matrix ρ , the dissipator superoperator $\mathcal{D}[c](\rho) = c\rho c^\dagger - \{c^\dagger c, \rho\}/2$ and the resonator photon loss rate κ . Using (18), the average fidelity of the i SWAP and $\sqrt{i$ SWAP gates as a function of the gate time is given by

$$\bar{F} = \frac{1}{10} [2 + (1+x)(1+2xy+y^2)], \quad (19)$$

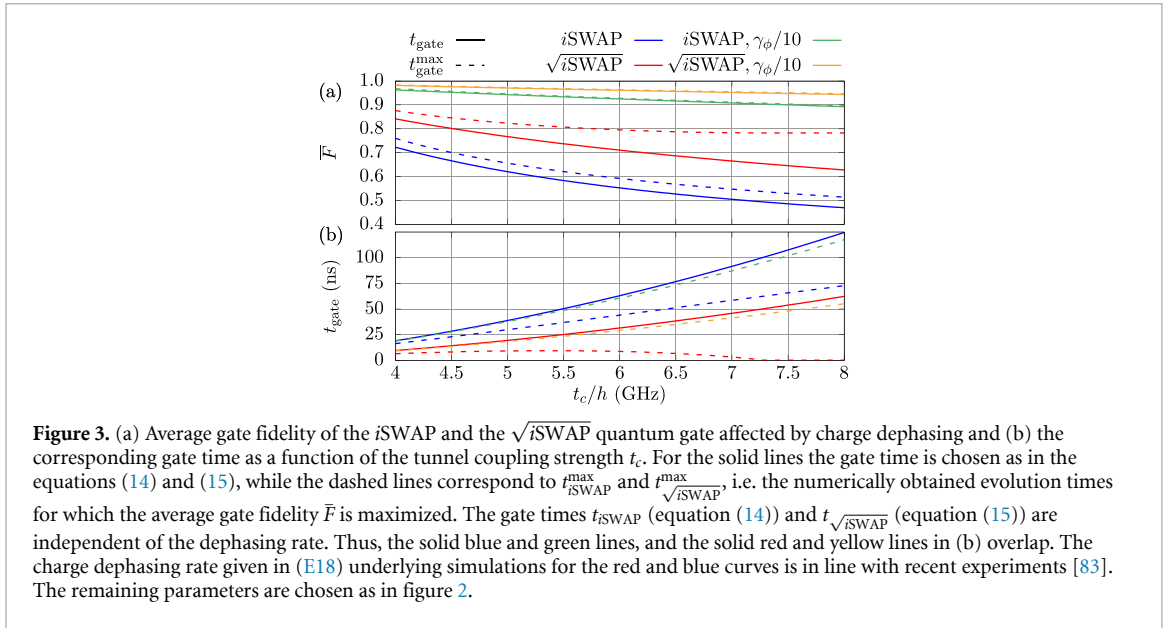
with $y = \exp\{-t \frac{\kappa g_c^2}{(\omega_c - 2t_c)^2}\}$ and $x = \sin(|g_{\text{eff}}|t)$ for the i SWAP gate and $x = \sin(|g_{\text{eff}}|t + \pi/4)$ for the $\sqrt{i$ SWAP gate. The average gate fidelity for both gates is presented in figure 2 as a function of the tunnel coupling strength t_c with which the resonator-DQD detuning is controlled. If the system is operated deep in the dispersive regime characterized by $|2t_c - \omega_c| \gg g_c$, e.g. as in [83], the decay rate in (18) can be as small as 20 kHz resulting in an average gate fidelity exceeding 99%. Resonator losses have the largest impact on the average gate fidelity at the resonance $2t_c = \omega_c$. This is not surprising because there is strong charge-photon hybridization at the resonance and, therefore, the gate is more susceptible to photon losses. The higher gate fidelity of the $\sqrt{i$ SWAP gate compared to the i SWAP gate can be attributed to the difference in the gate times, i.e. $2t_{\sqrt{i\text{SWAP}}} = t_{i\text{SWAP}}$.

4.2. Charge qubit dephasing

Qubit dephasing tends to be the limiting factor for the coherence of charge qubits. According to the detailed derivation presented in appendix D, charge qubit dephasing is described by the master equation

$$\dot{\rho} = -i[H, \rho] + \frac{\gamma_\phi(t_c)}{2} \sum_{i=1}^2 \mathcal{D} \left[(1 + \alpha_1) \tau_z^{(i)} + \alpha_2 \left(1 + \tau_+^{(1)} \tau_-^{(2)} + \tau_-^{(1)} \tau_+^{(2)} \right) \right] (\rho), \quad (20)$$

where the explicit definitions of the coefficients α_1 and α_2 in terms of the system parameters are listed in appendix D. As explained in detail in appendix E, the charge dephasing rate $\gamma_\phi(t_c)$ at the charge-noise sweet spot ($\epsilon = 0$) is inversely proportional to the tunnel coupling strength, $\gamma_\phi \propto 1/t_c$, with a reported value of $\gamma_\phi/(2\pi) = 9.9$ MHz for $2t_c/h = 19.2$ GHz [83]. When writing the explicit form of the dissipator in (20), one finds terms $\mathcal{O}(\alpha_i^0)$, terms $\propto \alpha_i \propto g_c^2$, and terms $\propto \alpha_i \alpha_j \propto g_c^4$ with $i, j \in \{1, 2\}$. In line with (18) we consider the terms $\mathcal{O}(g_c^2)$, while the terms $\mathcal{O}(g_c^4)$ are neglected in the following. We point out that keeping the $\mathcal{O}(g_c^4)$



terms would require including higher order corrections in the transformation (D1) because these corrections can give rise to additional terms $\mathcal{O}(g_c^4)$ in (20).

As the next step, (20) is employed to calculate the average gate fidelity for the i SWAP and the \sqrt{i} SWAP gate,

$$\bar{F}_{i\text{SWAP}} = \frac{1}{20} [7 + 3y_\gamma^2 - 2y_\gamma \cos(\beta t) + 8xy_\gamma z], \quad (21)$$

$$\bar{F}_{\sqrt{i}\text{SWAP}} = \frac{1}{20} \left[7 + 3y_\gamma^2 + 4y_\gamma |g_{\text{eff}}| \frac{\sin(\beta t)}{\beta} + 8xy_\gamma z \right], \quad (22)$$

with $y_\gamma = \exp\{-\gamma_\phi(t_c)(1 + 2\alpha_1)t\}$, $\beta = \sqrt{4g_{\text{eff}}^2 - \gamma_\phi^2(t_c)(1 + 2\alpha_1)^2}$, and $z = \cosh(\gamma_\phi(t_c)\alpha_2 t)$.

Figure 3(a) shows the average fidelity of the i SWAP and \sqrt{i} SWAP gates as a function of the tunnel coupling strength t_c . The blue (red) line gives the average gate fidelity for the evolution time set to $t_{i\text{SWAP}}$ (14) ($t_{\sqrt{i}\text{SWAP}}$ (15)) for which the respective gate is realized in the absence of decoherence processes according to (16) ((17)). The dashed lines, however, show the maximum gate fidelity for the specific set of system parameters obtained by maximizing the gate fidelity as a function of the evolution time. The green (yellow) line was obtained by assuming a charge dephasing rate an order of magnitude smaller than the values achieved in recent experiments. A comparison between the evolution time for which maximal gate fidelity $t_{i\text{SWAP}}^{\text{max}}$ ($t_{\sqrt{i}\text{SWAP}}^{\text{max}}$) is achieved and $t_{i\text{SWAP}}$ ($t_{\sqrt{i}\text{SWAP}}$) is presented in figure 3(b).

Figure 3(a) unveils that charge dephasing reduces the gate fidelity in the dispersive regime significantly. Due to the scaling $\gamma_\phi(t_c) \propto 1/t_c$, the dephasing rate increases with a decreasing tunnel coupling strength. However, the figure shows a reduction of the average gate fidelity with rising tunnel coupling strength. A closer look at the gate times as a function of the tunnel coupling strength presented in figure 3(b) provides an explanation for this observation: Increasing the tunnel coupling strength results in a longer gate time such that the system experiences charge dephasing at a reduced rate for a longer time period, whereby the longer gate time outweighs the benefits of a reduced dephasing rate. Moreover, figure 3(b) demonstrates that the maximal gate fidelity is achieved for evolution times shorter than the gate time in the ideal decoherence free scenario, $t_{i\text{SWAP}}$ ($t_{\sqrt{i}\text{SWAP}}$).

Analyzing figure 3 for a specific value of the tunnel coupling strength t_c unveils a higher average fidelity of the \sqrt{i} SWAP gate than the i SWAP gate. This property can again be attributed to the difference in gate time.

Inspecting the red dashed lines in figure 3, one observes an initially surprising behavior. In the highly dispersive regime with $t_c/h \gtrsim 7.25$ GHz, the average gate fidelity approaches a steady value while the gate time goes to zero. A vanishing gate time implies that the initial state $|\psi_0\rangle$ is not altered in any way, i.e. the map \mathcal{E} introduced in appendix B acts on the initial state as $\mathcal{E}(|\psi\rangle\langle\psi|) = |\psi\rangle\langle\psi|$. In this case, according to (B3), the average gate fidelity for the \sqrt{i} SWAP gate amounts to

$$\bar{F}(\mathcal{E}, U(t_{\sqrt{i}\text{SWAP}}, 0)) = \frac{1}{2} + \frac{\sqrt{2}}{5} \approx 0.78. \quad (23)$$

This result agrees with the value to which the red dashed line in figure 3(a) converges. The above reasoning allows us to conclude that an average gate fidelity of the $\sqrt{i\text{SWAP}}$ gate exceeding the ‘initial value’ of 0.78 for $t > 0$ requires $(d\bar{F}_{\sqrt{i\text{SWAP}}}/dt)|_{t=0} \neq 0$. This condition is fulfilled for

$$|g_{\text{eff}}| > \frac{(1 + \sqrt{2})(1 + 2\alpha_1)}{2} \gamma_\phi(t_c). \quad (24)$$

The comparison of the figures 2 and 3 shows that, in the dispersive regime, charge dephasing is the dominant decoherence mechanism.

At first sight, our results suggest an increased fidelity in the case that the coupling between the qubits and the resonator is closer to the resonance. On resonance, however, the realization of the $i\text{SWAP}$ or the $\sqrt{i\text{SWAP}}$ gate by simultaneously coupling two identical charge qubits to a resonator is not possible as explained in the following. In the resonant regime, the system is described by the Hamiltonian

$$H_{\text{res}} = g_c \sum_{i=1}^2 \left(\tau_+^{(i)} a + \tau_-^{(i)} a^\dagger \right), \quad (25)$$

in a rotating reference frame with respect to $\sum_{i=1}^2 t_c \tau_z^{(i)}$ and with the RWA applied. This Hamiltonian generates the time evolution

$$U_{\text{res}}(t) = \exp(-iH_{\text{res}}t), \quad (26)$$

which reduces to

$$U_{\text{res}}^{0p}(t) = P_0 U_{\text{res}}(t) P_0 = \begin{pmatrix} \frac{1}{3} [2 + \cos(\sqrt{6}g_c t)] & 0 & 0 & 0 \\ 0 & \cos^2\left(\frac{g_c}{\sqrt{2}}t\right) & -\sin^2\left(\frac{g_c}{\sqrt{2}}t\right) & 0 \\ 0 & -\sin^2\left(\frac{g_c}{\sqrt{2}}t\right) & \cos^2\left(\frac{g_c}{\sqrt{2}}t\right) & 0 \\ 0 & 0 & 0 & 1 \end{pmatrix}, \quad (27)$$

within the zero-photon subspace corresponding to the projection operator $P_0 = |0\rangle\langle 0|$. The generally non-vanishing matrix elements connecting the zero-photon subspace to states with higher photon numbers are

$$\begin{aligned} \langle -, -, 1 | U_{\text{res}}(t) | -, +, 0 \rangle &= \langle -, -, 1 | U_{\text{res}}(t) | +, -, 0 \rangle \\ &= -i \sin\left(\sqrt{2}g_c t\right) / \sqrt{2}, \end{aligned} \quad (28)$$

$$\begin{aligned} \langle -, +, 1 | U_{\text{res}}(t) | +, +, 0 \rangle &= \langle +, -, 1 | U_{\text{res}}(t) | +, +, 0 \rangle \\ &= -i \sin\left(\sqrt{6}g_c t\right) / \sqrt{6}, \end{aligned} \quad (29)$$

$$\langle -, -, 2 | U_{\text{res}}(t) | +, +, 0 \rangle = -\frac{2\sqrt{2}}{3} \sin^2\left(\frac{\sqrt{3}g_c}{\sqrt{2}}t\right). \quad (30)$$

A closer look unveils that there is no evolution time except $t = 0$ for which the matrix elements (28)–(30) vanish simultaneously, indicating an unavoidable leakage from the zero photon subspace to states with higher photon numbers, and thus implementing a quantum gate restricted to the zero photon subspace is not feasible in the resonant regime.

5. Conclusion

We demonstrated that a microwave resonator mediates a long-range interaction between two charge qubits defined in two spatially separated Si DQDs, each hosting a single charge carrier, either an electron or a hole, while being dispersively coupled to the same resonator mode. We found that this interaction can be harnessed to implement both the $i\text{SWAP}$ and the $\sqrt{i\text{SWAP}}$ two-qubit quantum gate within a gate time in the range of a few nanoseconds.

Detailed discussions of the most prominent noise sources, i.e. resonator photon losses and charge qubit dephasing, have shown that in the dispersive regime, charge dephasing is the dominant decoherence mechanism. Assuming a state-of-the-art resonator decay rate and charge qubit dephasing rate, the predicted average gate fidelities are below 90%. However, a reduction of the charge qubit dephasing rate by one order

of magnitude is predicted to result in gate fidelities surpassing 95%. Such a reduction is a plausible scenario in the near future, as understanding the origin of charge noise –the primary cause of charge and spin dephasing– is an active field of research [96, 97]. This ongoing research has already led to promising approaches to mitigate charge noise [98–100].

Data availability statement

The data cannot be made publicly available upon publication because they are not available in a format that is sufficiently accessible or reusable by other researchers. The data that support the findings of this study are available upon reasonable request from the authors.

Acknowledgments

J M and G B acknowledge the support by ARO Grant No. W911NF-15-1-0149.

Appendix A. Schrieffer–Wolff–Transformation to eliminate excited resonator states

The dynamics of the system consisting of two charge qubits coupled to a single mode of a microwave resonator is captured by the Hamiltonian $H = H_c + \sum_{i=1}^2 H_{\text{DQD}}^{(i)} + H_{\text{int}}^{(i)}$, with $H_{\text{DQD}}^{(i)} = \frac{\Omega^{(i)}}{2} \tau_z^{(i)}$ and $H_{\text{int}}^{(i)} = g_c(a + a^\dagger)(\sin \theta^{(i)} \tau_x^{(i)} + \cos \theta^{(i)} \tau_z^{(i)})$. In order to decouple the dynamics of the zero-photon subspace from the excited resonator states, we first divide H into a diagonal part $H_0 = H_c + \sum_{i=1}^2 H_{\text{DQD}}^{(i)}$, and an off-diagonal part $V = V_d + V_{\text{od}}$ [101]. Using the projectors $P_0 = |0\rangle\langle 0|$ and $Q_0 = 1 - P_0$, the block diagonal and block off-diagonal parts of V can be obtained as

$$V_d = P_0 V P_0 + Q_0 V Q_0, \quad (\text{A1})$$

$$V_{\text{od}} = P_0 V Q_0 + Q_0 V P_0. \quad (\text{A2})$$

Next, one can apply a Schrieffer–Wolff transformation with antihermitian generator S to find the effective Hamiltonian

$$\bar{H} = e^S H e^{-S}. \quad (\text{A3})$$

Here, we follow the perturbative approach $S = S_1 + S_2 + \dots$, with $S_n \sim V^n$ discussed in [101], allowing for the decoupling of the subspaces with different photon numbers up to a desired order in V . The first two contributions to the generator S , S_1 and S_2 , must obey the relations [101],

$$[H_0, S_1] = V_{\text{od}}, \quad (\text{A4})$$

$$[H_0, S_2] = -[V_d, S_1]. \quad (\text{A5})$$

Then, the effective Hamiltonian in the invariant subspace of P_0 , up to second order in the perturbation V , reads

$$\bar{H}_d = H_0 P_0 + P_0 V P_0 + \frac{1}{2} P_0 [S_1, V_{\text{od}}] P_0. \quad (\text{A6})$$

In general, an operator X transforms under the transformation generated by S as

$$\begin{aligned} e^S X e^{-S} &= \sum_{j=0}^{\infty} \frac{1}{j!} [X, -S]^{(j)} \\ &\approx X - [X, S_1] - [X, S_2] + \frac{1}{2} [X, S_1]^{(2)}, \end{aligned} \quad (\text{A7})$$

where the second line describes the contributions up to second order in the perturbation V and $[A, B]^{(j)} = [\dots [A, \underbrace{B, B}_{j\text{-times}}, \dots B]$.

In the general case of distinct qubits, i.e. $\varepsilon^{(1)} \neq \varepsilon^{(2)}$ and $t_c^{(1)} \neq t_c^{(2)}$, the equations (A4) and (A5) are solved by

$$\begin{aligned} S_1 = & \sum_{i=1}^2 \frac{g_c \sin \theta^{(i)}}{\omega_c + \Omega^{(i)}} \left(|1\rangle \langle 0| \tau_+^{(i)} - |0\rangle \langle 1| \tau_-^{(i)} \right) \\ & + \sum_{i=1}^2 \frac{g_c \sin \theta^{(i)}}{\omega_c - \Omega^{(i)}} \left(|1\rangle \langle 0| \tau_-^{(i)} - |0\rangle \langle 1| \tau_+^{(i)} \right) \\ & + \sum_{i=1}^2 \frac{g_c \cos \theta^{(i)}}{\omega_c} (|1\rangle \langle 0| - |0\rangle \langle 1|) \tau_z^{(i)}, \end{aligned} \quad (\text{A8})$$

and

$$\begin{aligned} S_2 = & \sqrt{2} |0\rangle \langle 2| \left(\sum_{i=1}^2 \frac{g_c^2 \cos^2 \theta^{(i)}}{2\omega_c^2} + \tau_z \sigma_z \frac{g_c^2 \cos \theta^{(1)} \cos \theta^{(2)}}{\omega_c^2} + \sum_{i=1}^2 \frac{1 + \tau_z^{(i)}}{2} \frac{g_c^2 \sin^2 \theta^{(i)}}{2\omega_c (\omega_c - \Omega^{(i)})} \right. \\ & + \sum_{i=1}^2 \frac{1 - \tau_z^{(i)}}{2} \frac{g_c^2 \sin^2 \theta^{(i)}}{2\omega_c (\omega_c + \Omega^{(i)})} - \sum_{i=1}^2 \tau_-^{(i)} \frac{g_c^2 \Omega^{(i)} \cos \theta^{(i)} \sin \theta^{(i)}}{\omega_c (2\omega_c + \Omega^{(i)}) (\omega_c + \Omega^{(i)})} - \sum_{i=1}^2 \tau_+^{(i)} \frac{g_c^2 \Omega^{(i)} \cos \theta^{(i)} \sin \theta^{(i)}}{\omega_c (2\omega_c - \Omega^{(i)}) (\omega_c - \Omega^{(i)})} \\ & + \sum_{i=1}^2 \tau_-^{(i)} \tau_-^{(j \neq i)} \frac{g_c^2 \sin \theta^{(i)} \sin \theta^{(j \neq i)}}{(\omega_c + \Omega^{(i)}) (\omega_c + \Omega^{(j \neq i)})} + \sum_{i=1}^2 \tau_-^{(i)} \tau_+^{(j \neq i)} \frac{g_c^2 \sin \theta^{(i)} \sin \theta^{(j \neq i)}}{(\omega_c + \Omega^{(i)}) (\omega_c - \Omega^{(j \neq i)})} \\ & \left. + \sum_{i=1}^2 \tau_+^{(i)} \tau_z^{(j \neq i)} \frac{g_c^2 \sin \theta^{(i)} \cos \theta^{(j \neq i)}}{\omega_c (\omega_c - \Omega^{(i)})} + \sum_{i=1}^2 \tau_-^{(i)} \tau_z^{(j \neq i)} \frac{g_c^2 \sin \theta^{(i)} \cos \theta^{(j \neq i)}}{\omega_c (\omega_c + \Omega^{(i)})} \right) - \text{h.c.}, \end{aligned} \quad (\text{A9})$$

respectively.

Given the above expression for S_1 , it is straightforward to determine the explicit form of the effective Hamiltonian \bar{H}_d (A6) up to second order in the perturbation V ,

$$\begin{aligned} \bar{H}_d = & \sum_{i=1}^2 \frac{E^{(i)}}{2} \tau_z^{(i)} + g_{\text{eff}} \tau_x^{(1)} \tau_x^{(2)} + g_1 \tau_z^{(1)} \tau_z^{(2)} \\ & + \sum_{i=1}^2 g_2^{(i)} \tau_x^{(i)} + \sum_{i=1}^2 g_3^{(i)} \tau_z^{(i)} \tau_x^{(j \neq i)}, \end{aligned} \quad (\text{A10})$$

up to an unimportant constant term that is neglected here. The coefficients are given by

$$g_{\text{eff}} = g_c^2 \sin \theta^{(1)} \sin \theta^{(2)} \sum_{i=1}^2 \frac{\omega_c}{\omega_c^2 - (\Omega^{(i)})^2}, \quad (\text{A11})$$

$$E^{(i)} = \Omega^{(i)} - \frac{g_c^2 \sin^2 \theta^{(i)}}{\omega_c - \Omega^{(i)}} + \frac{g_c^2 \sin^2 \theta^{(i)}}{\omega_c + \Omega^{(i)}}, \quad (\text{A12})$$

$$g_1 = -\frac{2g_c^2 \cos \theta^{(1)} \cos \theta^{(2)}}{\omega_c}, \quad (\text{A13})$$

$$g_2^{(i)} = \frac{g_c^2 \Omega^{(i)} \cos \theta^{(i)} \sin \theta^{(i)}}{\omega_c^2 - (\Omega^{(i)})^2}, \quad (\text{A14})$$

$$g_3^{(i)} = g_c^2 \cos \theta^{(i)} \sin \theta^{(j \neq i)} \left(\frac{1}{\omega_c} + \frac{\omega_c}{\omega_c^2 - (\Omega^{(i)})^2} \right). \quad (\text{A15})$$

To arrive at the equations (9)–(11) in the main text, identical qubits operated at the charge noise sweet spot $\varepsilon^{(i)} = 0$ are considered. In particular, this implies $\cos \theta^{(i)} = 0$ and $\sin \theta^{(i)} = 1$ as well as $\Omega^{(i)} = 2t_c$ for $i = 1, 2$. We note that the presence of the ZZ interaction in equation (A10) is unfavorable for the implementation of the two-qubit gates discussed in the main text (see also [102]). However, the explicit expression for the associated coupling strength, g_1 (A13), provides a solution to this issue. When operating the qubits at the charge noise sweet spot with $\varepsilon^{(i)} = 0$, one finds that g_1 vanishes. Additionally, near the charge noise sweet spot, the ZZ interaction is strongly suppressed as $g_1 \propto \varepsilon^{(1)} \varepsilon^{(2)}$. Furthermore, operating at the charge noise sweet spot maximizes the desired effective coupling g_{eff} between the two qubits.

We note that the perturbative approach underlying the derivation of (A10) requires $|g_c \sin \theta^{(i)}| \ll |\Omega^{(i)} - \omega_c|, |\Omega^{(i)} + \omega_c|$. Hence, \bar{H}_d is not valid in parameter domains with $\Omega^{(i)} \approx \omega_c$ where the qubits are close to resonance with the resonator mode.

Appendix B. Fidelity

Given the desired time evolution $|\psi\rangle\langle\psi| \rightarrow U|\psi\rangle\langle\psi|U^\dagger$ of a quantum system and the real implementation described by the map $|\psi\rangle\langle\psi| \rightarrow \mathcal{E}(|\psi\rangle\langle\psi|)$, we can measure the deviation of the real implementation from the ideal one by calculating the fidelity [103],

$$F = |\langle\psi|U^\dagger\mathcal{E}(|\psi\rangle\langle\psi|)U|\psi\rangle|. \quad (\text{B1})$$

However, this measure depends explicitly on the choice of the quantum state $|\psi\rangle$. To avoid the state dependency, one can define the *average fidelity* \bar{F} obtained by averaging over the fidelity of all possible quantum states,

$$\bar{F}(\mathcal{E}, U) = \int \langle\psi|U^\dagger\mathcal{E}(|\psi\rangle\langle\psi|)U|\psi\rangle d\psi. \quad (\text{B2})$$

In [93] it is demonstrated, that, in a d -dimensional Hilbert space, the average fidelity can be calculated by choosing a basis U_j/\sqrt{d} of $d \times d$ matrices, which form an orthonormal basis with respect to the Hilbert–Schmidt scalar product,

$$\bar{F}(\mathcal{E}, U) = \frac{\sum_j \text{tr}(U U_j^\dagger U^\dagger \mathcal{E}(U_j)) + d^2}{d^2(d+1)}. \quad (\text{B3})$$

Here, the Hilbert space is four-dimensional and spanned by the basis states $\{|0\rangle = |+, +\rangle, |1\rangle = |+, -\rangle, |2\rangle = |-, +\rangle, |3\rangle = |-, -\rangle\}$. Hence, the orthonormal set of matrices can be chosen as $X^k Z^l$ with $k, l = 0, 1, 2, 3, X|j\rangle \equiv |j+1 \pmod{4}\rangle$ and $Z|j\rangle \equiv e^{ij\pi/2}|j\rangle$.

Appendix C. Resonator damping

The resonator field $\propto (a + a^\dagger)$ couples to an external electromagnetic environment. In order to capture the impact of this coupling to the environment on the system dynamics, we first note that, according to (A7), $(a + a^\dagger)$ transforms to the reference frame set by the SW transformation up to first order in the perturbation V as,

$$\begin{aligned} a + a^\dagger &\rightarrow a + a^\dagger - \sum_{i=1}^2 \frac{g_c \sin\theta^{(i)}}{\omega_c + \Omega^{(i)}} \left[(|0\rangle\langle 0| - |1\rangle\langle 1| + \sqrt{2}|2\rangle\langle 0|) \tau_+^{(i)} + (|0\rangle\langle 0| - |1\rangle\langle 1| + \sqrt{2}|0\rangle\langle 2|) \tau_-^{(i)} \right] \\ &- \sum_{i=1}^2 \frac{g_c \sin\theta^{(i)}}{\omega_c - \Omega^{(i)}} \left[(|0\rangle\langle 0| - |1\rangle\langle 1| + \sqrt{2}|2\rangle\langle 0|) \tau_-^{(i)} + (|0\rangle\langle 0| - |1\rangle\langle 1| + \sqrt{2}|0\rangle\langle 2|) \tau_+^{(i)} \right] \\ &- \sum_{i=1}^2 \frac{g_c \cos\theta^{(i)}}{\omega_c} (2|0\rangle\langle 0| - 2|1\rangle\langle 1| + \sqrt{2}|2\rangle\langle 0| + \sqrt{2}|0\rangle\langle 2|) \tau_z^{(i)}. \end{aligned} \quad (\text{C1})$$

We aim at deriving a Lindblad master equation that includes the interaction of the system with the electromagnetic environment in the equation of motion for the system density matrix. Following the derivation of the Lindblad master equation outlined in [104], the electromagnetic environment is traced out, and subsequently the Born–Markov and secular approximations are applied. Moreover, we assume that the environment can be approximated to be at zero temperature, such that processes increasing the system energy due to the interaction with the environment are not allowed. As a result, the impact of the environment on the system dynamics can be described by the dissipators,

$$\mathcal{D}[a](\bar{\rho}), \quad (\text{C2})$$

$$\mathcal{D} \left[- \sum_{i=1}^2 \frac{g_c \sin\theta^{(i)}}{\omega_c + \Omega^{(i)}} (|1\rangle\langle 1| - |0\rangle\langle 0|) \tau_-^{(i)} - \sum_{i=1}^2 \frac{g_c \sin\theta^{(i)}}{\omega_c - \Omega^{(i)}} (|0\rangle\langle 0| - |1\rangle\langle 1|) \tau_-^{(i)} \right] (\bar{\rho}), \quad (\text{C3})$$

$$\mathcal{D} \left[- \sum_{i=1}^2 \frac{g_c \sin\theta^{(i)}}{\omega_c + \Omega^{(i)}} \sqrt{2}|0\rangle\langle 2| \tau_-^{(i)} \right] (\bar{\rho}), \quad (\text{C4})$$

$$\left\{ \begin{array}{l} \mathcal{D} \left[-\sum_{i=1}^2 \frac{g_c \sin \theta^{(i)}}{\omega_c - \Omega^{(i)}} \sqrt{2} |2\rangle \langle 0| \tau_-^{(i)} \right] (\bar{\rho}) \text{ if } 2\omega_c < \Omega^{(i)} \\ \mathcal{D} \left[-\sum_{i=1}^2 \frac{g_c \sin \theta^{(i)}}{\omega_c - \Omega^{(i)}} \sqrt{2} |0\rangle \langle 2| \tau_+^{(i)} \right] (\bar{\rho}) \text{ if } 2\omega_c > \Omega^{(i)} \end{array} \right\}, \quad (\text{C5})$$

$$\mathcal{D} \left[-2 \sum_{i=1}^2 \frac{g_c \cos \theta^{(i)}}{\omega_c} (|0\rangle \langle 0| - |1\rangle \langle 1|) \right] (\bar{\rho}), \quad (\text{C6})$$

$$\mathcal{D} \left[-\sum_{i=1}^2 \frac{g_c \cos \theta^{(i)}}{\omega_c} (\sqrt{2} |0\rangle \langle 2|) \tau_z^{(i)} \right] (\bar{\rho}), \quad (\text{C7})$$

where $\bar{\rho}$ is the density matrix in the reference frame set by the SW transformation.

Next, we note that the effective Hamiltonian \bar{H}_d (9) does not involve any coupling between subspaces with different photon numbers. Furthermore, the dissipators (C2)–(C7) do not describe processes increasing the resonator photon number in the system parameter regime characterized by $2\omega_c > \Omega^{(i)}$. These two observations lead to the following conclusion: if the system is initialized in the zero photon subspace and $2\omega_c > \Omega^{(i)}$, as considered in the main part of this paper, the system remains in the zero photon subspace during evolution. Thus, given this situation, among the dissipators (C2)–(C7) only,

$$\mathcal{D} \left[\sum_{i=1}^2 \left(\frac{g_c \sin \theta^{(i)}}{\omega_c + \Omega^{(i)}} - \frac{g_c \sin \theta^{(i)}}{\omega_c - \Omega^{(i)}} \right) |0\rangle \langle 0| \tau_-^{(i)} \right] (\bar{\rho}), \quad (\text{C8})$$

and

$$\mathcal{D} \left[-2 \sum_{i=1}^2 \frac{g_c \cos \theta^{(i)}}{\omega_c} |0\rangle \langle 0| \tau_z^{(i)} \right] (\bar{\rho}), \quad (\text{C9})$$

are not vanishing when acting on the system density matrix $\bar{\rho}$. The above dissipators remain unchanged under the transformation to the rotating reference frame in which the Hamiltonian H (12) is expressed.

Assuming identical qubits operated at the charge noise sweet spot ($\varepsilon = 0 \rightarrow \theta = \pi/2$) and taking into account that $\omega_c - \Omega^{(i)} \ll \omega_c + \Omega^{(i)}$ results in the dissipator used in equation (18) of the main text.

Appendix D. Qubit dephasing

Considering charge qubits, charge noise, i.e. random electric fields that occur at the position of the QD, is the dominating noise source. In semiconductors, low frequency charge noise with a noise spectral density that scales (approximately) inversely proportional to frequency ($1/f$) is typically observed. Fluctuations of the level detuning ε are the dominant effect of charge noise on charge qubits. According to (6) this translates directly to a fluctuation in the charge qubit energy Ω . This in turn implies that a charge qubit couples to charge noise via the operator τ_z . Here, two spatially separated charge qubits are considered such that the charge noise acting on the individual qubits can be assumed to be independent and uncorrelated. In the following, identical qubits are assumed, i.e. $\theta^{(1)} = \theta^{(2)} = \theta$ and $\Omega^{(1)} = \Omega^{(2)} = \Omega$. Then, according to (A7), the respective coupling operator $\tau_z^{(i)}$ transforms to the reference frame set by the SW-transformation up to second order in the perturbation V as,

$$\begin{aligned} \tau_z^{(i)} &\rightarrow (1 + \alpha_1 (|1\rangle \langle 1| + |0\rangle \langle 0|)) \tau_z^{(i)} \\ &\quad - 2 \frac{g_c \sin \theta^{(i)}}{\omega_c + \Omega^{(i)}} (|1\rangle \langle 0| \tau_+^{(i)} + |0\rangle \langle 1| \tau_-^{(i)}) \\ &\quad + 2 \frac{g_c \sin \theta^{(i)}}{\omega_c - \Omega^{(i)}} (|1\rangle \langle 0| \tau_-^{(i)} + |0\rangle \langle 1| \tau_+^{(i)}) \\ &\quad + \alpha_2 (1 + \tau_-^{(1)} \tau_+^{(2)} + \tau_+^{(1)} \tau_-^{(2)}) (|0\rangle \langle 0| - |1\rangle \langle 1|) \\ &\quad + \alpha_3 \tau_z^{(j \neq i)} \tau_x^{(i)} (|0\rangle \langle 0| - |1\rangle \langle 1|) \\ &\quad + \alpha_4 \tau_x^{(i)} (|1\rangle \langle 1| + |0\rangle \langle 0|) \\ &\quad + \alpha_5 (\sqrt{2} |2\rangle \langle 0| - \sqrt{2} |0\rangle \langle 2|) (\tau_+^{(1)} \tau_-^{(2)} - \tau_-^{(1)} \tau_+^{(2)}) \end{aligned}$$

$$\begin{aligned}
& + \alpha_6 \left(\sqrt{2}|0\rangle\langle 2|\tau_-^{(1)}\tau_-^{(2)} + \sqrt{2}|2\rangle\langle 0|\tau_+^{(1)}\tau_+^{(2)} \right) \\
& + \alpha_7 \left(\sqrt{2}|0\rangle\langle 2|\tau_+^{(1)}\tau_+^{(2)} + \sqrt{2}|2\rangle\langle 0|\tau_-^{(1)}\tau_-^{(2)} \right) \\
& + \alpha_8 \left(\sqrt{2}|0\rangle\langle 2|\tau_+^{(2)}\frac{1+\tau_z^{(1)}}{2} + \sqrt{2}|2\rangle\langle 0|\tau_-^{(2)}\frac{1+\tau_z^{(1)}}{2} \right) \\
& + \alpha_9 \left(\sqrt{2}|0\rangle\langle 2|\tau_-^{(2)}\frac{1-\tau_z^{(1)}}{2} + \sqrt{2}|2\rangle\langle 0|\tau_+^{(2)}\frac{1-\tau_z^{(1)}}{2} \right) \\
& + \alpha_{10} \left(\sqrt{2}|0\rangle\langle 2|\tau_-^{(2)}\frac{1+\tau_z^{(1)}}{2} + \sqrt{2}|2\rangle\langle 0|\tau_+^{(2)}\frac{1+\tau_z^{(1)}}{2} \right) \\
& + \alpha_{11} \left(\sqrt{2}|0\rangle\langle 2|\tau_+^{(2)}\frac{1-\tau_z^{(1)}}{2} + \sqrt{2}|2\rangle\langle 0|\tau_-^{(2)}\frac{1-\tau_z^{(1)}}{2} \right), \tag{D1}
\end{aligned}$$

with

$$\alpha_1 = -\frac{g_c^2 \sin^2 \theta}{(\omega_c - \Omega)^2} - \frac{g_c^2 \sin^2 \theta}{(\omega_c + \Omega)^2}, \tag{D2}$$

$$\alpha_2 = -\frac{g_c^2 \sin^2 \theta}{(\omega_c - \Omega)^2} + \frac{g_c^2 \sin^2 \theta}{(\omega_c + \Omega)^2}, \tag{D3}$$

$$\alpha_3 = -\frac{g_c^2 \sin \theta \cos \theta}{\omega_c (\omega_c - \Omega)} + \frac{g_c^2 \sin \theta \cos \theta}{\omega_c (\omega_c + \Omega)}, \tag{D4}$$

$$\alpha_4 = +\frac{g_c^2 \sin \theta \cos \theta}{\omega_c (\omega_c - \Omega)} + \frac{g_c^2 \sin \theta \cos \theta}{\omega_c (\omega_c + \Omega)}, \tag{D5}$$

$$\alpha_5 = \frac{2g_c^2 \sin^2 \theta}{\Omega^2 - \omega_c^2}, \tag{D6}$$

$$\alpha_6 = \frac{2g_c^2 \sin^2 \theta}{(\omega_c + \Omega)^2}, \tag{D7}$$

$$\alpha_7 = -\frac{2g_c^2 \sin^2 \theta}{(\omega_c - \Omega)^2}, \tag{D8}$$

$$\alpha_8 = -\frac{4g_c^2 \cos \theta \sin \theta}{\omega_c (2\omega_c - \Omega)}, \tag{D9}$$

$$\alpha_9 = -\frac{4g_c^2 \cos \theta \sin \theta}{\omega_c (2\omega_c + \Omega)}, \tag{D10}$$

$$\alpha_{10} = \frac{2g_c^2 \sin 2\theta}{(\omega_c + \Omega)(2\omega_c + \Omega)}, \tag{D11}$$

$$\alpha_{11} = \frac{2g_c^2 \sin 2\theta}{(\omega_c - \Omega)(2\omega_c - \Omega)}. \tag{D12}$$

Now, we proceed as explained in appendix C. Given the low-frequency character of charge noise, only processes conserving the system energy are supported, so that charge noise is accounted for by the dissipator,

$$\mathcal{D} \left[(1 + \alpha_1) \tau_z^{(i)} - \alpha_2 \left(1 + \tau_-^{(1)} \tau_+^{(2)} + \tau_+^{(1)} \tau_-^{(2)} \right) (|1\rangle\langle 1| - |0\rangle\langle 0|) \right] (\bar{\rho}), \tag{D13}$$

whereby $\omega_c \neq \Omega^{(i)}$ and $\Omega^{(1)} = \Omega^{(2)}$ is assumed. Applying the same reasoning as in appendix E, the dissipator simplifies to,

$$\mathcal{D} \left[(1 + \alpha_1) \tau_z^{(i)} + \alpha_2 \left(1 + \tau_-^{(1)} \tau_+^{(2)} + \tau_+^{(1)} \tau_-^{(2)} \right) |0\rangle\langle 0| \right] (\bar{\rho}), \tag{D14}$$

if the system is initialized in the zero photon subspace. The above dissipator remains unchanged under the transformation to the rotating reference frame in which the Hamiltonian H (12) is expressed.

Appendix E. Charge dephasing rate

In order to determine the charge dephasing rate, we first consider a general qubit Hamiltonian $\tilde{H}(\varepsilon)$ that depends on a quantity ε subjected to noise. Let us now define the unitary operator $U(\varepsilon)$ that transforms

$\tilde{H}(\varepsilon)$ to its eigenbasis, i.e.

$$H(\varepsilon) = U(\varepsilon) \tilde{H}(\varepsilon) U^\dagger(\varepsilon) = \frac{\omega(\varepsilon)}{2} \tau_z, \quad (\text{E1})$$

where $\omega(\varepsilon)/2\pi$ is the qubit transition frequency. Now, suppose that the unperturbed Hamiltonian is given for $\varepsilon = \varepsilon_0$. Then, the Hamiltonian for a general ε in the eigenbasis of the unperturbed Hamiltonian reads,

$$H(\varepsilon) = U(\varepsilon_0) \tilde{H}(\varepsilon) U^\dagger(\varepsilon_0). \quad (\text{E2})$$

As the next step, we expand $H(\varepsilon)$ about the unperturbed value $\varepsilon = \varepsilon_0$ up to second order,

$$H(\varepsilon) = H(\varepsilon_0) + \left. \frac{dH(\varepsilon)}{d\varepsilon} \right|_{\varepsilon_0} \delta\varepsilon + \frac{1}{2} \left. \frac{d^2H(\varepsilon)}{d\varepsilon^2} \right|_{\varepsilon_0} \delta\varepsilon^2 + \mathcal{O}(\delta\varepsilon^3) \quad (\text{E3})$$

$$= \frac{1}{2} [(\omega(\varepsilon_0) + \delta\omega_z) \tau_z + \delta\omega_x \tau_x + \delta\omega_y \tau_y], \quad (\text{E4})$$

where $\delta\varepsilon = \varepsilon - \varepsilon_0$. Equation (E4) follows from a decomposition of equation (E3) into factors multiplying the Pauli operators. A thorough analysis reveals that the parameters can be calculated as follows,

$$\delta\omega_z = \left. \frac{d\omega(\varepsilon)}{d\varepsilon} \right|_{\varepsilon_0} \delta\varepsilon + \frac{1}{2} \left. \frac{d^2\omega(\varepsilon)}{d\varepsilon^2} \right|_{\varepsilon_0} \delta\varepsilon^2, \quad (\text{E5})$$

$$\begin{aligned} \delta\omega_x = \Re \left[\langle g(\varepsilon_0) | \left(\left. \frac{d\tilde{H}(\varepsilon)}{d\varepsilon} \right|_{\varepsilon_0} \right) | e(\varepsilon_0) \rangle \right] \delta\varepsilon \\ + \frac{1}{2} \Re \left[\langle g(\varepsilon_0) | \left(\left. \frac{d^2\tilde{H}(\varepsilon)}{d\varepsilon^2} \right|_{\varepsilon_0} \right) | e(\varepsilon_0) \rangle \right] \delta\varepsilon^2, \end{aligned} \quad (\text{E6})$$

$$\begin{aligned} \delta\omega_y = \Im \left[\langle g(\varepsilon_0) | \left(\left. \frac{d\tilde{H}(\varepsilon)}{d\varepsilon} \right|_{\varepsilon_0} \right) | e(\varepsilon_0) \rangle \right] \delta\varepsilon \\ + \frac{1}{2} \Im \left[\langle g(\varepsilon_0) | \left(\left. \frac{d^2\tilde{H}(\varepsilon)}{d\varepsilon^2} \right|_{\varepsilon_0} \right) | e(\varepsilon_0) \rangle \right] \delta\varepsilon^2, \end{aligned} \quad (\text{E7})$$

with $|g(\varepsilon_0)\rangle$ and $|e(\varepsilon_0)\rangle$ the ground state and the excited state of the unperturbed Hamiltonian $\tilde{H}(\varepsilon_0)$, respectively.

Given a Hamiltonian of the form (E4), assuming Gaussian distributed noise with zero mean and a power spectral density $S_\varepsilon(\tilde{\omega}) = A_\varepsilon/|\tilde{\omega}|$ with constant A_ε , as typically observed for charge noise, a Ramsey free-induction decay sequence will lead to a Gaussian decay $\propto \exp[-(t/T_\phi)^2]$ with dephasing time [105],

$$T_\phi = \left[\frac{1}{2} \left(\left. \frac{d\omega(\varepsilon)}{d\varepsilon} \right|_{\varepsilon_0} \right)^2 A_\varepsilon \log(r) + \frac{1}{4} \left(\left. \frac{d^2\omega(\varepsilon)}{d\varepsilon^2} \right|_{\varepsilon_0} \right)^2 A_\varepsilon^2 \log^2(r) \right]^{-\frac{1}{2}}, \quad (\text{E8})$$

with $r = \frac{\omega_U}{\omega_R}$, where ω_U and ω_R are cutoff frequencies $\omega_U \leq \tilde{\omega} \leq \omega_R$ that are not relevant for the reasoning in this manuscript.

Here, the qubit Hamiltonian $\tilde{H}(\varepsilon)$ is given by the DQD Hamiltonian \tilde{H}_{DQD} (equation (1)). This Hamiltonian depends on two parameters, ε and t_c , both susceptible to charge noise. However, the effect of charge noise on the tunnel coupling strength t_c is often negligible compared to that on the level detuning ε [85]. Thus, only the level detuning is considered as a fluctuating parameter in the following. Following the above reasoning, we find

$$\omega(\varepsilon) = \sqrt{\varepsilon^2 + (2t_c)^2}, \quad (\text{E9})$$

$$\delta\omega_z = \frac{\varepsilon_0}{\omega(\varepsilon_0)} \delta\varepsilon + \frac{1}{2} \left(\frac{1}{\omega(\varepsilon_0)} - \frac{\varepsilon_0^2}{\omega(\varepsilon)^3} \right) \delta\varepsilon^2, \quad (\text{E10})$$

$$\delta\omega_x = -\frac{t_c}{\omega(\varepsilon_0)} \delta\varepsilon, \quad (\text{E11})$$

$$\delta\omega_y = 0. \quad (\text{E12})$$

Equation (E10) shows that the first-order fluctuations of the qubit energy splitting can be suppressed by operating the system at the charge noise sweet spot characterized by $\varepsilon_0 = 0$. Setting the system to this particular configuration, one has

$$\omega(\varepsilon_0 = 0) = 2t_c, \quad (\text{E13})$$

$$\delta\omega_z = \frac{1}{2} \frac{1}{2t_c} \delta\varepsilon^2, \quad (\text{E14})$$

$$\delta\omega_x = -\frac{1}{2} \delta\varepsilon, \quad (\text{E15})$$

and

$$T_\phi = 2\pi \left[\frac{1}{4} \left(\frac{1}{2t_c} \right)^2 A_\varepsilon^2 \log^2(r) \right]^{-\frac{1}{2}}. \quad (\text{E16})$$

Given the above expression for the dephasing time it follows that the dephasing rate,

$$\gamma_\phi = \frac{2\pi}{T_\phi} \propto \frac{1}{t_c}, \quad (\text{E17})$$

is inversely proportional to the tunnel coupling strength t_c . In a recent experiment, a charge dephasing rate of $\gamma_\phi/2\pi = 9.9$ MHz with the tunnel coupling strength set to $2t_c/h = 19.2$ GHz was observed [83]. According to equation (E17), the reported values allow us to infer the proportionality factor C between the charge dephasing rate γ_ϕ and the inverse tunnel coupling strength $1/t_c$,

$$\frac{\gamma_\phi(t_c)}{2\pi} = \frac{C}{t_c}, \quad (\text{E18})$$

with $C = 393 \mu\text{eV} \times \text{MHz}$. The dephasing rate given in equation (E18) is employed in the calculations in section 4.2 of the main text. We note that a master equation of the form,

$$\dot{\rho}^\tau(t) = -i[t_c\tau_z, \rho^\tau(t)] + \frac{\gamma_\phi}{2} \mathcal{D}[\tau_z] \rho^\tau(t), \quad (\text{E19})$$

where the dephasing rate $\gamma_\phi = 2\pi/T_\phi$ describes an exponential decay $\propto \exp[-t/T_\phi]$ of the coherences of the charge qubit density matrix $\rho^\tau(t)$ of an individual charge qubit, while the discussion in this appendix predicts a Gaussian decay. We point out that $\exp[-t/T_\phi] \leq \exp[-(t/T_\phi)^2]$ in the time domain $0 \leq t \leq T_\phi$. Thus, on this timescale, the master equation description overestimates the impact of charge noise on charge dephasing. As the gate times in the main text are shorter than the charge dephasing time, it is guaranteed that the impact of charge noise is not underestimated in our calculations.

ORCID iDs

Florian Kayatz  <https://orcid.org/0009-0005-3572-3561>

Jonas Mielke  <https://orcid.org/0000-0002-8097-5099>

Guido Burkard  <https://orcid.org/0000-0001-9053-2200>

References

- [1] Zajac D M, Hazard T M, Mi X, Wang K and Petta J R 2015 A reconfigurable gate architecture for Si/SiGe quantum dots *Appl. Phys. Lett.* **106** 223507
- [2] Zajac D M, Hazard T M, Mi X, Nielsen E and Petta J R 2016 Scalable gate architecture for a one-dimensional array of semiconductor spin qubits *Phys. Rev. Appl.* **6** 054013
- [3] Sigillito A J, Loy J C, Zajac D M, Gullans M J, Edge L F and Petta J R 2019 Site-selective quantum control in an isotopically enriched $^{28}\text{Si}/\text{Si}_{0.7}\text{Ge}_{0.3}$ quadruple quantum dot *Phys. Rev. Appl.* **11** 061006
- [4] Volk C et al 2019 Loading a quantum-dot based ‘Qubyte’ register *npj Quantum Inf.* **5** 29
- [5] Lawrie W I L et al 2020 Quantum dot arrays in silicon and germanium *Appl. Phys. Lett.* **116** 080501
- [6] Loss D and DiVincenzo D P 1998 Quantum computation with quantum dots *Phys. Rev. A* **57** 120–6
- [7] Burkard G, Ladd T D, Pan A, Nichol J M and Petta J R 2023 Semiconductor spin qubits *Rev. Mod. Phys.* **95** 025003
- [8] Boross P, Széchenyi G, Culcer D and Pályi A 2016 Control of valley dynamics in silicon quantum dots in the presence of an interface step *Phys. Rev. B* **94** 035438
- [9] Schoenfield J S, Freeman B M and Jiang H 2017 Coherent manipulation of valley states at multiple charge configurations of a silicon quantum dot device *Nat. Commun.* **8** 64
- [10] Stockklauser A, Scarlino P, Koski J V, Gasparinetti S, Andersen C K, Reichl C, Wegscheider W, Ihn T, Ensslin K and Wallraff A 2017 Strong coupling cavity QED with gate-defined double quantum dots enabled by a high impedance resonator *Phys. Rev. X* **7** 011030

- [11] Hendrickx N W, Lawrie W I L, Petit L, Sammak A, Scappucci G and Veldhorst M 2020 A single-hole spin qubit *Nat. Commun.* **11** 3478
- [12] Gorman J, Hasko D G and Williams D A 2005 Charge-Qubit operation of an isolated double quantum dot *Phys. Rev. Lett.* **95** 090502
- [13] Petersson K D, Petta J R, Lu H and Gossard A C 2010 Quantum coherence in a one-electron semiconductor charge qubit *Phys. Rev. Lett.* **105** 246804
- [14] Dovzhenko Y, Stehlik J, Petersson K D, Petta J R, Lu H and Gossard A C 2011 Nonadiabatic quantum control of a semiconductor charge qubit *Phys. Rev. B* **84** 161302
- [15] Shi Z et al 2013 Coherent quantum oscillations and echo measurements of a Si charge qubit *Phys. Rev. B* **88** 075416
- [16] Yang Y-C, Coppersmith S N and Friesen M 2019 Achieving high-fidelity single-qubit gates in a strongly driven charge qubit with $1/f$ charge noise *npj Quantum Inf.* **5** 12
- [17] Benito M, Croot X, Adelsberger C, Putz S, Mi X, Petta J R and Burkard G 2019 Electric-field control and noise protection of the flopping-mode spin qubit *Phys. Rev. B* **100** 125430
- [18] Croot X, Mi X, Putz S, Benito M, Borjans F, Burkard G and Petta J R 2020 Flopping-mode electric dipole spin resonance *Phys. Rev. Res.* **2** 012006
- [19] Mutter P M and Burkard G 2021 Natural heavy-hole flopping mode qubit in germanium *Phys. Rev. Res.* **3** 013194
- [20] Barthel C, Reilly D J, Marcus C M, Hanson M P and Gossard A C 2009 Rapid single-shot measurement of a singlet-triplet qubit *Phys. Rev. Lett.* **103** 160503
- [21] Barthel C, Medford J, Marcus C M, Hanson M P and Gossard A C 2010 Interlaced dynamical decoupling and coherent operation of a singlet-triplet qubit *Phys. Rev. Lett.* **105** 266808
- [22] Maune B M et al 2012 Coherent singlet-triplet oscillations in a silicon-based double quantum dot *Nature* **481** 344–7
- [23] Takeda K, Noiri A, Yoneda J, Nakajima T and Tarucha S 2020 Resonantly driven singlet-triplet spin qubit in silicon *Phys. Rev. Lett.* **124** 117701
- [24] Jirovec D et al 2021 A singlet-triplet hole spin qubit in planar Ge *Nat. Mater.* **20** 1106–12
- [25] Jirovec D et al 2022 Dynamics of hole singlet-triplet qubits with large g -factor differences *Phys. Rev. Lett.* **128** 126803
- [26] DiVincenzo D P 1995 Two-bit gates are universal for quantum computation *Phys. Rev. A* **51** 1015–22
- [27] Schuch N and Siewert J 2003 Natural two-qubit gate for quantum computation using the XY interaction *Phys. Rev. A* **67** 032301
- [28] Imamoglu A, Awschalom D D, Burkard G, DiVincenzo D P, Loss D, Sherwin M and Small A 1999 Quantum information processing using quantum dot spins and cavity qed *Phys. Rev. Lett.* **83** 4204–7
- [29] Blais A, Huang R-S, Wallraff A, Girvin S M and Schoelkopf R J 2004 Cavity quantum electrodynamics for superconducting electrical circuits: an architecture for quantum computation *Phys. Rev. A* **69** 062320
- [30] Rasmussen S E and Zinner N T 2020 Simple implementation of high fidelity controlled-*iswap* gates and quantum circuit exponentiation of non-hermitian gates *Phys. Rev. Res.* **2** 033097
- [31] Córcoles A D, Magesan E, Srinivasan S J, Cross A W, Steffen M, Gambetta J M and Chow J M 2015 Demonstration of a quantum error detection code using a square lattice of four superconducting qubits *Nat. Commun.* **6** 6979
- [32] Debnath S, Linke N M, Figgatt C, Landsman K A, Wright K and Monroe C 2016 Demonstration of a small programmable quantum computer with atomic qubits *Nature* **536** 63–66
- [33] Fujisawa T, Shinkai G, Hayashi T and Ota T 2011 Multiple two-qubit operations for a coupled semiconductor charge qubit *Physica E* **43** 730–4
- [34] Shulman M D, Dial O E, Harvey S P, Bluhm H, Umansky V and Yacoby A 2012 Demonstration of entanglement of electrostatically coupled singlet-triplet qubits *Science* **336** 202–5
- [35] Li H-O, Cao G, Yu G-D, Xiao M, Guo G-C, Jiang H-W and Guo G-P 2015 Conditional rotation of two strongly coupled semiconductor charge qubits *Nat. Commun.* **6** 7681
- [36] Nichol J M, Orona L A, Harvey S P, Fallahi S, Gardner G C, Manfra M J and Yacoby A 2017 High-fidelity entangling gate for double-quantum-dot spin qubits *npj Quantum Inf.* **3** 3
- [37] Neyens S F et al 2019 Measurements of capacitive coupling within a quadruple-quantum-dot array *Phys. Rev. Appl.* **12** 064049
- [38] Cayao J, Benito M and Burkard G 2020 Programmable two-qubit gates in capacitively coupled flopping-mode spin qubits *Phys. Rev. B* **101** 195438
- [39] Veldhorst M et al 2015 A two-qubit logic gate in silicon *Nature* **526** 410–4
- [40] Zajac D M, Sigillito A J, Russ M, Borjans F, Taylor J M, Burkard G and Petta J R 2018 Resonantly driven CNOT gate for electron spins *Science* **359** 439–42
- [41] Watson T F et al 2018 A programmable two-qubit quantum processor in silicon *Nature* **555** 633–7
- [42] Huang W et al 2019 Fidelity benchmarks for two-qubit gates in silicon *Nature* **569** 532–6
- [43] Xue X, Watson T F, Helsen J, Ward D R, Savage D E, Lagally M G, Coppersmith S N, Eriksson M A, Wehner S and Vandersypen L M K 2019 Benchmarking gate fidelities in a Si/SiGe two-qubit device *Phys. Rev. X* **9** 021011
- [44] Taylor J M, Engel H-A, Dür W, Yacoby A, Marcus C M, Zoller P and Lukin M D 2005 Fault-tolerant architecture for quantum computation using electrically controlled semiconductor spins *Nat. Phys.* **1** 177–83
- [45] Li X, Barnes E, Kestner J P and Das Sarma S 2017 Intrinsic errors in transporting a single-spin qubit through a double quantum dot *Phys. Rev. A* **96** 012309
- [46] Flentje H, Mortemousque P-A, Thalineau R, Ludwig A, Wieck A D, Bäuerle C and Meunier T 2017 Coherent long-distance displacement of individual electron spins *Nat. Commun.* **8** 501
- [47] Fujita T, Baart T A, Reichl C, Wegscheider W and Vandersypen L M K 2017 Coherent shuttle of electron-spin states *npj Quantum Inf.* **3** 22
- [48] Feng M, Kwong C J, Koh T S and Kwek L C 2018 Coherent transfer of singlet-triplet qubit states in an architecture of triple quantum dots *Phys. Rev. B* **97** 245428
- [49] Zhao X and Hu X 2018 Toward high-fidelity coherent electron spin transport in a GaAs double quantum dot *Sci. Rep.* **8** 13968
- [50] Mills A R, Zajac D M, Gullans M J, Schupp F J, Hazard T M and Petta J R 2019 Shuttling a single charge across a one-dimensional array of silicon quantum dots *Nat. Commun.* **10** 1063
- [51] Ginzel F, Mills A R, Petta J R and Burkard G 2020 Spin shuttling in a silicon double quantum dot *Phys. Rev. B* **102** 195418
- [52] Krzywdka J A and Cywiński Łukasz 2020 Adiabatic electron charge transfer between two quantum dots in presence of $1/f$ noise *Phys. Rev. B* **101** 035303
- [53] Buonacorsi B, Shaw B and Baugh J 2020 Simulated coherent electron shuttling in silicon quantum dots *Phys. Rev. B* **102** 125406

- [54] Van Diepen C J, Hsiao T-K, Mukhopadhyay U, Reichl C, Wegscheider W and Vandersypen L M K 2021 Electron cascade for distant spin readout *Nat. Commun.* **12** 77
- [55] Krzywda J A and Cywiński Łukasz 2021 Interplay of charge noise and coupling to phonons in adiabatic electron transfer between quantum dots *Phys. Rev. B* **104** 075439
- [56] Yoneda J et al 2021 Coherent spin qubit transport in silicon *Nat. Commun.* **12** 4114
- [57] Noiri A, Takeda K, Nakajima T, Kobayashi T, Sammak A, Scappucci G and Tarucha S 2022 A shuttling-based two-qubit logic gate for linking distant silicon quantum processors *Nat. Commun.* **13** 5740
- [58] Boter J M et al 2022 Spiderweb array: a sparse spin-qubit array *Phys. Rev. Appl.* **18** 024053
- [59] Croot X G, Pauka S J, Watson J D, Gardner G C, Fallahi S, Manfra M J and Reilly D J 2018 Device architecture for coupling spin qubits via an intermediate quantum state *Phys. Rev. Appl.* **10** 044058
- [60] Malinowski F K et al 2018 Spin of a multielectron quantum dot and its interaction with a neighboring electron *Phys. Rev. X* **8** 011045
- [61] Malinowski F K et al 2019 Fast spin exchange across a multielectron mediator *Nat. Commun.* **10** 1196
- [62] Seidler I, Struck T, Xue R, Focke N, Trelenkamp S, Bluhm H and Schreiber L R 2022 Conveyor-mode single-electron shuttling in Si/SiGe for a scalable quantum computing architecture *npj Quantum Inf.* **8** 100
- [63] Wang Z et al 2023 Jellybean quantum dots in silicon for qubit coupling and on-chip quantum chemistry *Adv. Mater.* **35** 2208557
- [64] Langrock V, Krzywda J A, Focke N, Seidler I, Schreiber L R and Cywiński Łukasz 2023 Blueprint of a Scalable spin qubit shuttle device for coherent mid-range qubit transfer in disordered Si/SiGe/SiO₂ *PRX Quantum* **4** 020305
- [65] Kandel Y P, Qiao H, Fallahi S, Gardner G C, Manfra M J and Nichol J M 2021 Adiabatic quantum state transfer in a semiconductor quantum-dot spin chain *Nat. Commun.* **12** 2156
- [66] Greentree A D, Cole J H, Hamilton A R and Hollenberg L C L 2004 Coherent electronic transfer in quantum dot systems using adiabatic passage *Phys. Rev. B* **70** 235317
- [67] Petrosyan D, Nikolopoulos G M and Lambropoulos P 2010 State transfer in static and dynamic spin chains with disorder *Phys. Rev. A* **81** 042307
- [68] Chancellor N and Haas S 2012 Using the J_1 – J_2 quantum spin chain as an adiabatic quantum data bus *New J. Phys.* **14** 095025
- [69] Srinivasa V, Levy J and Hellberg C S 2007 Flying spin qubits: a method for encoding and transporting qubits within a dimerized Heisenberg spin- $\frac{1}{2}$ chain *Phys. Rev. B* **76** 094411
- [70] Farooq U, Bayat A, Mancini S and Bose S 2015 Adiabatic many-body state preparation and information transfer in quantum dot arrays *Phys. Rev. B* **91** 134303
- [71] Ban Y, Chen Xi, Kohler S and Platero G 2019 Spin entangled state transfer in quantum dot arrays: coherent adiabatic and speed-up protocols *Adv. Quantum Tech.* **2** 1900048
- [72] Picó-Cortés J, Gallego-Marcos F and Platero G 2019 Direct transfer of two-electron quantum states in ac-driven triple quantum dots *Phys. Rev. B* **99** 155421
- [73] Gullans M J and Petta J R 2020 Coherent transport of spin by adiabatic passage in quantum dot arrays *Phys. Rev. B* **102** 155404
- [74] Devoret M H and Schoelkopf R J 2013 Superconducting circuits for quantum information: an outlook *Science* **339** 1169–74
- [75] Blais A, Grimsmo A L, Girvin S M and Wallraff A 2021 Circuit quantum electrodynamics *Rev. Mod. Phys.* **93** 025005
- [76] Xiang Z-L, Ashhab S, You J Q and Nori F 2013 Hybrid quantum circuits: superconducting circuits interacting with other quantum systems *Rev. Mod. Phys.* **85** 623–53
- [77] Burkard G, Gullans M J, Mi X and Petta J R 2020 Superconductor–semiconductor hybrid-circuit quantum electrodynamics *Nat. Rev. Phys.* **2** 129–40
- [78] Benito M, Mi X, Taylor J M, Petta J R and Burkard G 2017 Input-output theory for spin-photon coupling in Si double quantum dots *Phys. Rev. B* **96** 235434
- [79] Mi X, Benito M, Putz S, Zajac D M, Taylor J M, Burkard G and Petta J R 2018 A coherent spin–photon interface in silicon *Nature* **555** 599–603
- [80] Samkharadze N, Zheng G, Kalhor N, Brousse D, Sammak A, Mendes U C, Blais A, Scappucci G and Vandersypen L M K 2018 Strong spin-photon coupling in silicon *Science* **359** 1123–7
- [81] Borjans F, Croot X G, Mi X, Gullans M J and Petta J R 2020 Resonant microwave-mediated interactions between distant electron spins *Nature* **577** 195–8
- [82] Harvey-Collard P, Dijkema J, Zheng G, Sammak A, Scappucci G and Vandersypen L M K 2022 Coherent spin-spin coupling mediated by virtual microwave photons *Phys. Rev. X* **12** 021026
- [83] Yu C X et al 2023 Strong coupling between a photon and a hole spin in silicon *Nat. Nanotechnol.* **18** 741–6
- [84] Van Woerkom D J et al 2018 Microwave photon-mediated interactions between semiconductor qubits *Phys. Rev. X* **8** 041018
- [85] Benito M, Petta J R and Burkard G 2019 Optimized cavity-mediated dispersive two-qubit gates between spin qubits *Phys. Rev. B* **100** 081412
- [86] Dijkema J, Xue X, Harvey-Collard P, Rimbach-Russ M, de Snoo S L, Zheng G, Sammak A, Scappucci G and Vandersypen L M K 2023 Two-qubit logic between distant spins in silicon (arXiv:2310.16805)
- [87] Scarlino P et al 2022 *In situ* tuning of the electric-dipole strength of a double-dot charge qubit: charge-noise protection and ultrastrong coupling *Phys. Rev. X* **12** 031004
- [88] DiCarlo L, Lynch H J, Johnson A C, Childress L I, Crockett K, Marcus C M, Hanson M P and Gossard A C 2004 Differential charge sensing and charge delocalization in a tunable double quantum dot *Phys. Rev. Lett.* **92** 226801
- [89] Lu W, Ji Z, Pfeiffer L, West K W and Rimbarg A J 2003 Real-time detection of electron tunnelling in a quantum dot *Nature* **423** 422–5
- [90] Colles J I, Mahoney A C, Hornibrook J M, Doherty A C, Lu H, Gossard A C and Reilly D J 2013 Dispersive readout of a few-electron double quantum dot with fast rf gate sensors *Phys. Rev. Lett.* **110** 046805
- [91] Scarlino P et al 2019 All-microwave control and dispersive readout of gate-defined quantum dot qubits in circuit quantum electrodynamics *Phys. Rev. Lett.* **122** 206802
- [92] Makhlin Y 2002 Nonlocal properties of two-qubit gates and mixed states and the optimization of quantum computations *Quantum Inf. Process.* **1** 243–52
- [93] Nielsen M A 2002 A simple formula for the average gate fidelity of a quantum dynamical operation *Phys. Lett. A* **303** 249–52
- [94] Wang K, Payette C, Dovzhenko Y, Deelman P W and Petta J R 2013 Charge relaxation in a single-electron Si/SiGe double quantum dot *Phys. Rev. Lett.* **111** 046801
- [95] Mi X, Cady J V, Zajac D M, Deelman P W and Petta J R 2017 Strong coupling of a single electron in silicon to a microwave photon *Science* **355** 156–8

- [96] Connors E J, Nelson J, Edge L F and Nichol J M 2022 Charge-noise spectroscopy of Si/SiGe quantum dots via dynamically-decoupled exchange oscillations *Nat. Commun.* **13** 940
- [97] Ye F, Ellaboudy A, Albrecht D, Vudatha R, Jacobson N T and Nichol J M 2024 Characterization of individual charge fluctuators in Si/SiGe quantum dots (arXiv:2401.14541)
- [98] Paquelet Wuetz B, Degli Esposti D, Zwerver A-M J, Amitonov S V, Botifoll M, Arbiol J, Vandersypen L M K, Russ M and Scappucci G 2023 Reducing charge noise in quantum dots by using thin silicon quantum wells *Nat. Commun.* **14** 1385
- [99] Elsayed A *et al* 2024 Low charge noise quantum dots with industrial CMOS manufacturing *npj Quantum Inf.* **10** 70
- [100] Ye F, Ellaboudy A and Nichol J M 2024 Stabilizing an individual charge fluctuator in a Si/SiGe quantum dot (arXiv:2407.05439)
- [101] Bravyi S, DiVincenzo D P and Loss D 2011 Schrieffer–Wolff transformation for quantum many-body systems *Ann. Phys., NY* **326** 2793–826
- [102] Moskalenko I N, Simakov I A, Abramov N N, Grigorev A A, Moskalev D O, Pishchimova A A, Smirnov N S, Zikiy E V, Rodionov I A and Besedin I S 2022 High fidelity two-qubit gates on fluxoniums using a tunable coupler *npj Quantum Inf.* **8** 130
- [103] Nielsen M A and Chuang I L 2010 *Quantum Computation and Quantum Information* 10th edn (Cambridge University Press)
- [104] Breuer H-P and Petruccione F 2007 *The Theory of Open Quantum Systems* (Oxford University Press)
- [105] Russ M and Burkard G 2015 Asymmetric resonant exchange qubit under the influence of electrical noise *Phys. Rev. B* **91** 235411